Electronic Structure and Spectroscopy of Nickel(II), Palladium(II), and Platinum(II) Acetylacetonate Complexes

Frederick D. Lewis,* Gwen D. Salvi, David R. Kanis, and Mark A. Ratner

Department of Chemistry, Northwestern University, Evanston, Illinois 60208-3113

Received September 4, 1992

The electronic structure and optical spectra of $Ni(acac)_2$ and $Pd(acac)_2$ have been investigated using the semiemperical INDO/S–SCF–CI (ZINDO) algorithm. The results of the electronic structure calculations are in good agreement with those of previous ab initio calculations for these complexes. Increasing the atomic number of the metal is found to increase the metal–ligand covalency, to increase the separation of the two highest occupied and two lowest unoccupied, ligand-localized (π and π^*) molecular orbitals, and to decrease the separation between the highest occupied and lowest unoccupied molecular orbitals. The effects of electronic relaxation (due to Coulomb and exchange integrals) and configuration interaction on the calculated energies of singlet–singlet transitions are analyzed using Platt diagrams to illustrate the origin of the d→d transitions, observed for $Ni(acac)_2$ but not for $Pd(acac)_2$ or $Pt(acac)_2$, and the increasing complexity of the ultraviolet portion of the spectrum with increasing atomic number. Thus the ZINDO calculations provide the basis for the first detailed rationalization of the complex optical spectra of the group 10(II) β-diketonates.

Introduction

The discovery that metal β-diketonates can be used as precursors for the thermal and photochemical production of homogeneous and heterogeneous catalysts[1-5] and for thin film metal–organic chemical vapor phase deposition (MOCVD)[6-8] has stimulated a revival of interest in the properties of these complexes. Our interest in the electronic structure and spectroscopy of the group 10(II) β-diketonates was attracted by the observation that irradiation of platinum(II) bis(β-diketonates) in the presence of hydrosilanes or olefins yields, sequentially, a highly reactive homogeneous hydrosilation catalyst and colloidal platinum.[5] An understanding of the primary photochemistry in these molecules requires an accurate description of their electronic structure and assignment of their optical spectra. However, in contrast to most metal-organic molecules where a qualitative description of optical transitions can be made rather easily, the assignment of the electronic transitions in the metal(II) β-diketonates is complicated by the number of possible electronic transitions these molecules may possess. Specifically, these d^8 systems can, in principle, possess low-lying ligand$_\sigma$-to-metal charge transfer (L_σMCT), ligand$_\pi$-to-metal charge transfer (L_πMCT), metal-to-ligand charge transfer (MLCT), intraligand (ligand-centered, e.g., $\pi\rightarrow\pi^*$), and ligand field metal "d→d") transitions. In their classical studies of the electronic absorption spectra of metal β-diketonates, Cotton and co-workers[9-12] assigned several weak low energy bands of square-planar Ni(II) β-diketonates to ligand field transitions and the lowest energy allowed transition to two nearly-degenerate ligand $\pi\rightarrow\pi^*$ excitations. However, the optical spectra of Pd(II) and Pt(II) β-diketonates were reported to be more complex and were not assigned.[9]

The extension of the semiempirical INDO/S–SCF–CI (hereafter referred to as ZINDO) model Hamiltonian to first- and second-row transition metal species by Zerner and co-workers,[13,14] makes possible the relatively facile calculation of electronic structure and optical spectra of symmetric transition metal complexes. We report here computational results obtained for $Ni(acac)_2$ and $Pd(acac)_2$ using the ZINDO algorithm. This chemically-oriented treatment allows us to trace the origins of electronic transitions and to compare them with the observed optical spectra. This analysis leads to a refinement of the assignment of Cotton and Wise[12] for the optical spectrum of $Ni(acac)_2$, to the first assignment for $Pd(acac)_2$, and, by extrapolation of these results, to the first assignment for $Pt(acac)_2$.

Experimental Section

Materials and Optical Spectra. Ultraviolet–visible absorption spectra were measured using a Hewlett-Packard 8452A diode-array spectrophotometer. Dichloromethane (Aldrich, spectrophotometric grade) was distilled over calcium hydride prior to use. Ethanol (Aldrich, reagent, denatured, spectrophotometric grade) was used as purchased. All metal(II) bis(acetylacetonates) [$M(acac)_2$] were purchased from Aldrich. $Ni(acac)_2$ was dried under vacuum at 80 °C overnight. $Pt(acac)_2$ was sublimed prior to use. $Pd(acac)_2$ was used as purchased.

Methods of Calculation. The calculations were performed using the INDO/S model of Zerner and co-workers.[13,14] This method includes the intermediate neglect of differential overlap (INDO)[15] adopted for spectroscopy (INDO/S)[16] and applied to transition-metal systems.[13,14,17] All self-consistent field (SCF) calculations were of the closed-shell restricted Hartree–Fock type (RHF). Excited states were generated using a single-excitation configuration–interaction (SECI) method. To describe the low-energy excited states accurately, 100 singly excited configurations were included in the SECI procedure. Oscillator strengths were calculated using the dipole length operator, retaining all one-center terms but omitting two-center contributions. One-center exchange integrals, which are necessary in accurately separating different terms within a configuration, are included in the calculation. The two-center Coulomb integrals were calculated using the Mataga–Nishimoto ex-

(1) Cullen, W. R.; Wickenheiser, E. B. *J. Organomet. Chem.* **1989**, *370*, 141–154.
(2) Belyakova, Z. V.; Knyazeva, L. K.; Chernyshev, E. A. *Zh. Obshch. Khim.* **1983**, *53*, 1591–1596.
(3) Rao, C. D.; Rase, H. F. *Ind. Eng. Chem. Prod. Res. Dev.* **1981**, *20*, 95–101.
(4) Oxman, J. D.; Boardman, L. D. Eur. Pat. Appl. EP 398,701, 1990.
(5) Lewis, F. D.; Salvi, G. D. Manuscript in preparation.
(6) Kodas, T. T.; Comita, P. B. *Acc. Chem. Res.* **1990**, *23*, 188–194.
(7) Mikami, N.; Ohki, R.; Kido, H. *Chem. Phys.* **1990**, *141*, 431–440.
(8) Klassen, R. B.; Baum, T. H. *Organometallics* **1989**, *8*, 2477–2482.
(9) Holm, R. H.; Cotton, F. A. *J. Am. Chem. Soc.* **1958**, *80*, 5658–5663.
(10) Cotton, F. A.; Fackler, J. P. *J. Am. Chem. Soc.* **1961**, *83*, 2818–2825.
(11) Cotton, F. A.; Harris, C. B.; Wise, J. J. *Inorg. Chem.* **1967**, *6*, 909–915.
(12) Cotton, F. A.; Wise, J. J. *Inorg. Chem.* **1967**, *6*, 917–924.
(13) Bacon, A. D.; Zerner, M. C. *Theoret. Chim. Acta* **1979**, *53*, 21–54.
(14) Zerner, M. C.; Loew, G. H.; Kirchner, R. F.; Mueller-Westerhoff, U. T. *J. Am. Chem. Soc.* **1980**, *102*, 589–599.
(15) Pople, J. A.; Beveridge, D. L.; Dobosh, P. A. *J. Chem. Phys.* **1967**, *47*, 2026.
(16) Ridley, J.; Zerner, M. *Theoret. Chim. Acta* **1973**, *32*, 111–134.
(17) Anderson, W. P.; Edwards, W. D.; Zerner, M. C. *Inorg. Chem.* **1986**, *25*, 2728–2732.

0020-1669/93/1332-1251$04.00/0

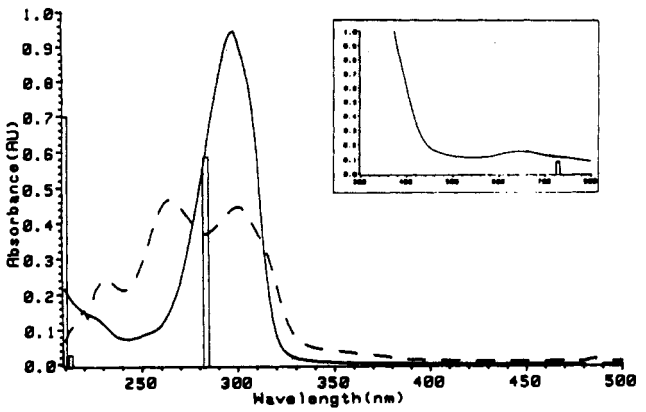

Figure 1. Electronic absorption spectra of 5×10^{-5} M $Ni(acac)_2$ in dichloromethane (- - -) and ethanol (—) solutions. Inset: 2×10^{-2} M ethanol solution. Vertical bars indicate calculated energies and oscillator strengths.

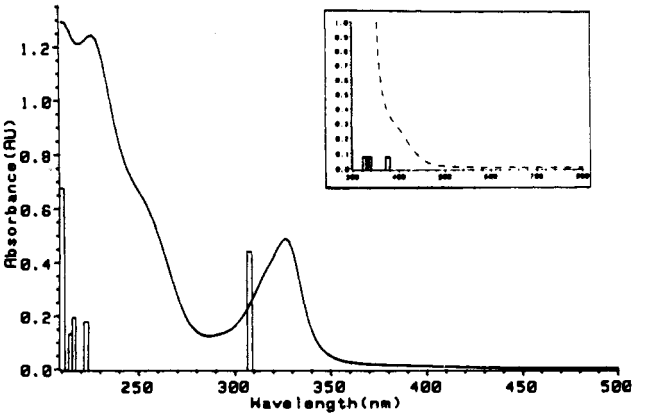

Figure 2. Electronic absorption spectrum of 5×10^{-5} M $Pd(acac)_2$ in ethanol solution. Inset: 2×10^{-2} M ethanol solution. Vertical bars indicate calculated energies and oscillator strengths.

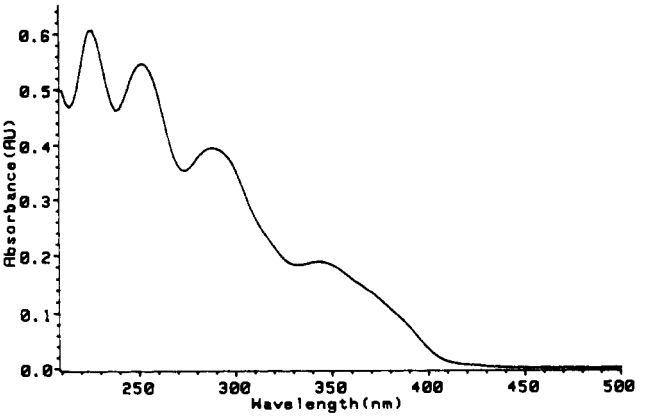

Figure 3. Electronic absorption spectrum of 5×10^{-5} M $Pt(acac)_2$ in ethanol solution.

pression.[18] The ZINDO parameterization scheme employed in this work was that described in the literature,[17] no parameters were modified to fit our experimental data. The nickel parameters were those used in a recent INDO/S study on $Ni(H_2O)_6^{2+}$.[17] Since INDO/S palladium parameters are currently unavailable, INDO/1 palladium parameters[19] were employed in this study.

The geometries for $Ni(acac)_2$[20] and $Pd(acac)_2$[21] were taken from X-ray crystal data and optimized to D_{2h} symmetry. Metal–oxygen (M–O) bond lengths were set at 2.02 Å. The z axis was set perpendicular to the plane, the x axis as the bisector of the O–M–O angles within the chelate rings, and the y axis as the bisector of the O–M–O angles between the acetylacetonate ligands. ZINDO calculations were also performed on the ligand acetylacetonate anion (acac) using the optimized ligand geometries of both $Ni(acac)_2$ and $Pd(acac)_2$. Only minor differences were found between the calculations using the two geometries. Each ZINDO calculation required approximately 5–15 min of CPU time on our local Stellar mini supercomputer.

Results and Discussion

Electronic Absorption Spectra. The absorption spectrum of acetylacetone in dichloromethane solution consists of a single maximum at 274 nm ($\epsilon = 8.8 \times 10^3$). As originally reported by Morton et al.,[22] addition of NaOH to acetylacetone in ethanol solution results in a shift of the absorption maximum to 292 nm and an increase in intensity ($\epsilon = 2 \times 10^4$–5×10^4). This spectrum was assigned to the chelated species. Holm and Cotton[9] attempted to group the acetylacetonate complexes of different metals according to the appearance of the absorption spectra. The first type of spectra was described as displaying a single symmetric absorption band in the ultraviolet region. This "class I" contained the alkali metal salts of the acetylacetonate anion, with maximum near 290 nm. The class II spectra also displayed one ultraviolet absorption band near 290 nm but with a shoulder on the long wavelength side. This group contained the majority of alkaline earth and transition metal complexes, including $Ni(acac)_2$ (Figure 1). The class III spectra, including that of $Cu(acac)_2$, contained the same asymmetric band as observed in the previous class but with an additional absorption band at higher energies. The ultraviolet spectra of $Pd(acac)_2$ (Figure 2) and $Pt(acac)_2$ (Figure 3) were described as being a "great deal richer" than that of the other β-diketonate complexes and, therefore, fit into none of the above classes.

Cotton and Fackler[10] attributed the solvent dependence of the ultraviolet spectrum of $Ni(acac)_2$ (Figure 1) to the presence of solvated monomeric square planar $Ni(acac)_2$ in coordinating solvents such as ethanol and a trimeric octahedral complex $[Ni(acac)_2]_3$ in noncoordinating solvents such as dichloromethane. The two β-diketonate ligands symmetrically chelate the central metal atom in a square planar fashion in $Pd(acac)_2$[21] and $Pt(acac)_2$[23] and in the pseudooctahedral $Ni(acac)_2 \cdot 2H_2O$,[24] as shown by X-ray crystallography. Cotton and co-workers assigned[10,12] the ultraviolet maximum of $Ni(acac)_2$ to two overlapping ligand $\pi \rightarrow \pi^*$ transitions and assigned the very weak absorption maxima at 635 nm, 1090 nm, and 1520 nm to d→d transitions. As shown in Figure 1, the spectrum of $Ni(acac)_2$ in ethanol solution displays maxima at 644 nm ($\epsilon = 8$), 298 nm ($\epsilon = 1.9 \times 10^4$), and a shoulder at 224 nm.

The ultraviolet spectra of $Pd(acac)_2$ and $Pt(acac)_2$ in ethanol solution are shown in Figures 2 and 3 and are essentially identical to those observed in noncoordinating solvents such as dichloromethane. The absence of solvent dependence is attributed to the existence of these complexes as "square planar monomers" in all solvents. The absorption spectrum of $Pd(acac)_2$ displays maxima at 326 nm ($\epsilon = 9.8 \times 10^3$) and 228 nm ($\epsilon = 2.5 \times 10^4$) and shoulders at 380 nm (Figure 2 inset) and 250 nm. The ultraviolet spectrum of $Pt(acac)_2$ (Figure 3) contains four well-defined absorption bands with maxima at 344 nm ($\epsilon = 3.9 \times 10^3$), 286 nm ($\epsilon = 7.9 \times 10^3$), 252 nm ($\epsilon = 1.1 \times 10^4$), and 226 nm ($\epsilon = 1.2 \times 10^4$). No absorption bands are observed at longer wavelengths for either $Pd(acac)_2$ or $Pt(acac)_2$.

(18) Mataga, N.; Nishimoto, K. *Z. Physik. Chem.* **1957**, *13*, 140.
(19) Anderson, W. P.; Cundari, T. R.; Drago, R. S.; Zerner, M. C. *Inorg. Chem.* **1990**, *29*, 1–3.
(20) Horrocks, W. D., Jr.; Templeton, D. H.; Zalkin, A. *Inorg. Chem.* **1968**, *7*, 1552–1557.
(21) (a) Knyazeva, A. N.; Shugam, E. A.; Shkol'nikova, L. M. *J. Struct. Chem. (Engl. Transl.)* **1971**, *11*, 875–876. (b) Burton, N. A.; Hillier, I. H.; Guest, M. F.; Kendrick, J. *Chem. Phys. Lett.* **1989**, *155*, 195–198.
(22) Morton, R. A.; Hassan, A.; Calloway, T. C. *J. Chem. Soc.* **1934**, 883–901.
(23) Onuma, S.; Horioka, K.; Inoue, H.; Shibata, S. *Bull. Chem. Soc. Jpn.* **1980**, *53*, 2679–2680.
(24) Montgomery, H.; Lingafelter, E. C. *Acta Crystallogr.* **1964**, *17*, 1481–1482.

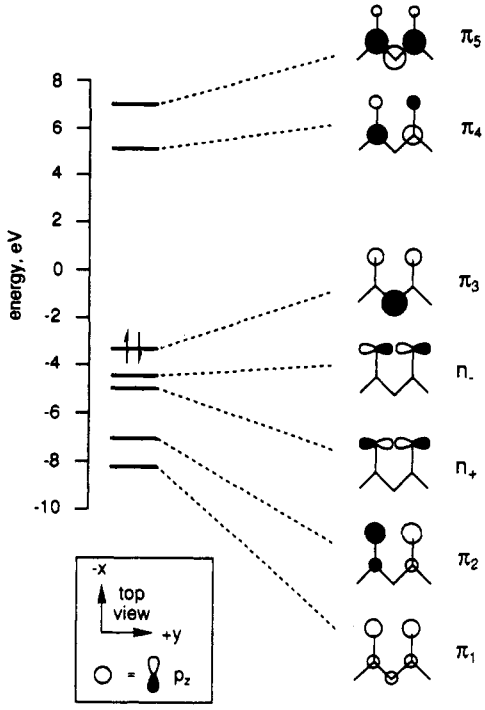

Figure 4. Frontier molecular orbitals and molecular orbital energies of the acetylacetonate anion. Electrons shown in the highest occupied molecular orbital.

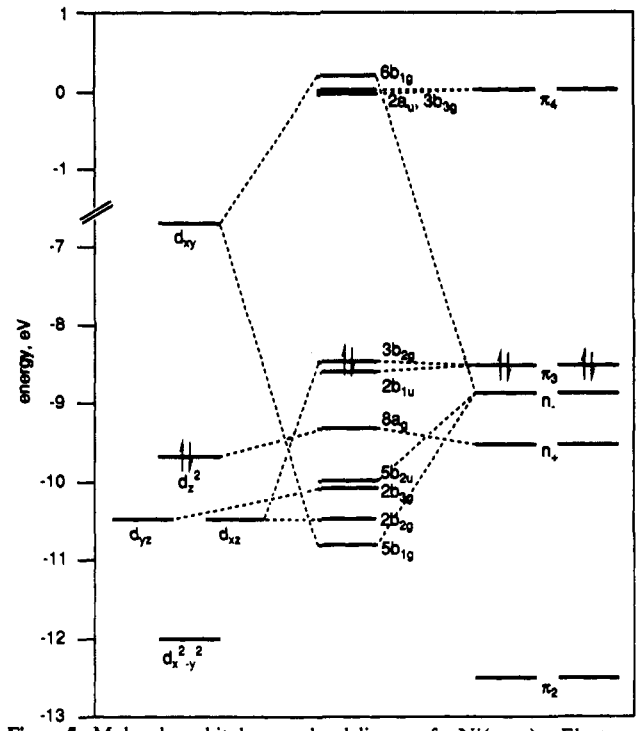

Figure 5. Molecular orbital energy level diagram for Ni(acac)$_2$. Electrons shown in the highest occupied molecular orbital.

Comparison of the absorption spectra of the group 10(II) β-diketonates (Figures 1–3), reveals two significant features: visible d→d absorption bands are observed only for nickel, and the complexity of the ultraviolet region increases for Ni < Pd < Pt. The "classical" explanation[25] for the former feature is that the HOMO and LUMO of the Ni complex are metal d orbitals which shift to energies below the highest occupied and above the lowest unoccupied ligand orbitals for the heavier metals. To our knowledge, no explanation for the latter feature has been postulated. In the following sections we will describe first how the electronic structure of the group 10(II) β-diketonates changes with the atomic number of the metal and then how these differences in electronic structure determine the appearance of the optical spectra.

Ground State Electronic Structures. The ZINDO-derived frontier molecular orbitals and molecular orbital energies of the acetylacetonate anion are shown pictorially in Figure 4. The frontier orbitals consist of five π-localized orbitals characteristic of a five-center, six electron p_z-orbital system and two occupied σ molecular orbitals arising from the antisymmetric (n_-) and symmetric (n_+) combinations of the oxygen lone pair p_y orbitals. The relative eigenvalues and eigenvectors for these orbitals are qualitatively similar to those previously derived from Hückel theory by Evans et al.[26]

The frontier molecular orbital energy level diagram for Ni(acac)$_2$ is shown in Figure 5 and the eigenvectors shown pictorially in Figure 6.[27] Since the ligation sphere about the metal atom consists of two acetylacetonate ligands far removed from one another, the (acac)$_2$ "fragment" in the metal(II) β-diketonates can be treated as the symmetric and antisymmetric combinations of the isolated acetylacetonate ligands. Ligand orbitals of gerade symmetry (e.g., the antisymmetric combination of π_3) interact with the nickel s- and d-orbitals while ligand orbitals of ungerade symmetry (e.g., the symmetric combination of π_3) interact with nickel p-orbitals. The ZINDO calculations indicate that many

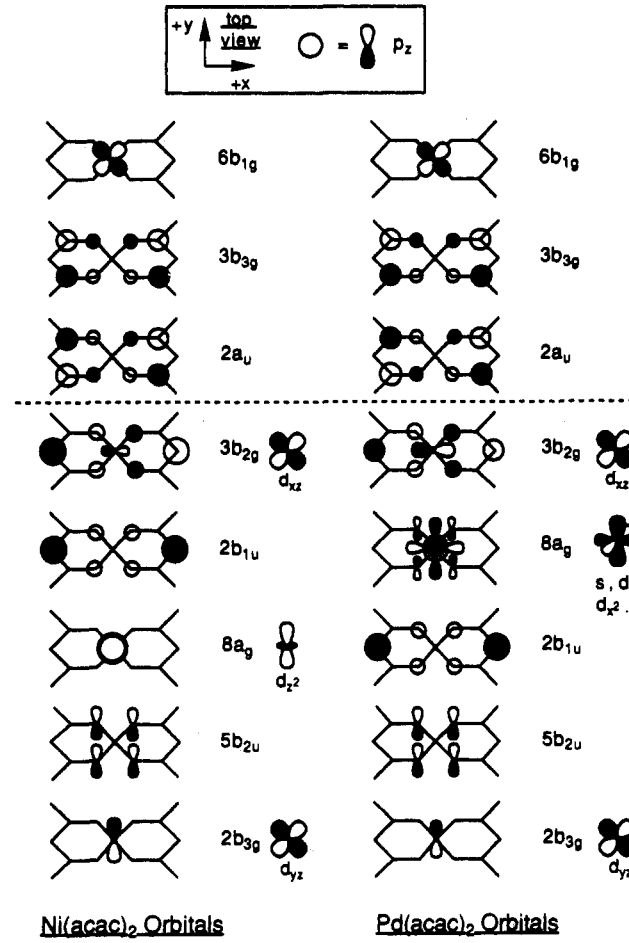

Figure 6. Frontier molecular orbitals of Ni(acac)$_2$ and Pd(acac)$_2$.

of the frontier orbitals in Ni(acac)$_2$ are localized on either the metal (e.g., $2b_{2g}$ and $2b_{3g}$) or on the ligand (e.g., $5b_{2u}$, $2b_{1u}$, $2a_u$, and $3b_{3g}$) (Figure 6). In other molecular orbitals, significant mixing of both metal and ligand orbitals is observed. For example, the interaction of the unoccupied nickel d_{xy} with the antisymmetric

(25) Mason, W. R.; Gray, H. B. *J. Am. Chem. Soc.* **1968**, *90*, 5721–5729.
(26) Evans, S.; Hamnett, A.; Orchard, A. F.; Lloyd, D. R. *Faraday Disc. Chem. Soc.* **1972**, *54*, 227–250.
(27) Tabular data found in supplementary material.

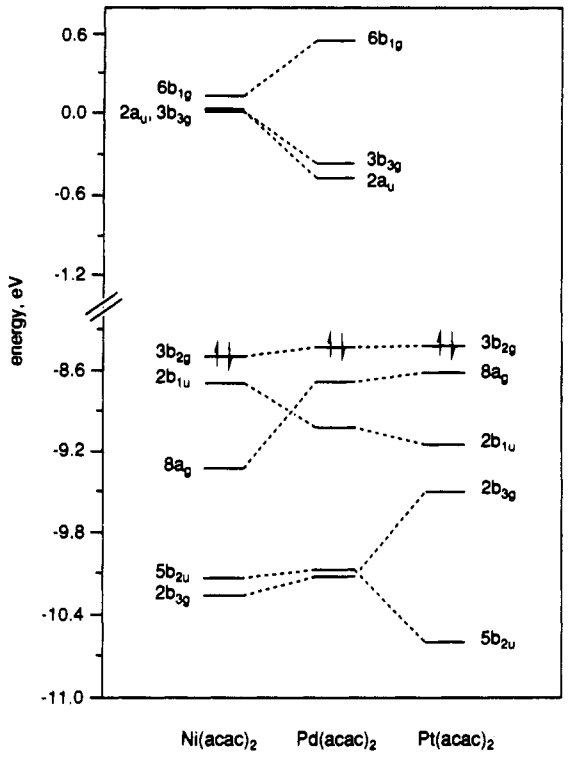

Figure 7. Correlation diagram between ZINDO-derived frontier occupied and unoccupied molecular orbital energies of $Ni(acac)_2$ and $Pd(acac)_2$ and relative PSHONDO-derived[30] occupied orbital energies of $Pt(acac)_2$ (see text). Electrons are shown in the highest occupied molecular orbital.

combination of ligand n_ lone pairs forms the occupied $5b_{1g}$ MO, which is responsible for σ-coordination, and the unoccupied $6b_{1g}$ MO. Mixing of the occupied nickel d_{xz} with the antisymmetric combination of the ligand π_3 orbitals results in the formation of the $2b_{2g}$ MO and $3b_{2g}$ HOMO. The HOMO in $Ni(acac)_2$ is localized (94%) on the ligand by virtue of the large (1.5 eV) splitting between the d_{xz} and π_3 orbitals.

The conclusion that both the two highest occupied and two lowest unoccupied orbitals of $Ni(acac)_2$ are ligand-localized stands in marked contrast with the "classical" electronic structure model[25] for group 10(II) complexes which display low energy d→d absorption bands and with the extended-Hückel calculations by Cotton and co-workers.[11] Our results are, however, in good qualitative agreement with the occupied molecular orbitals derived from ab initio SCF MO calculations of Hirota and Shibata[28] and the CNDO calculations of Fragalà et al.[29] The latter calculation, however, provides a different order for the ligand-localized orbitals than does the ZINDO calculation. The ZINDO-derived location of the highest occupied metal-localized orbital ($8a_g$) well below the ligand-localized HOMO ($3b_{2g}$) and SHOMO ($2b_{1u}$) is also consistent with a detailed analysis of the photoelectron spectrum.[29,30]

The ZINDO-derived eigenvalues and eigenvectors for $Pd(acac)_2$ are qualitatively similar to those for $Ni(acac)_2$.[27] However, the correlation diagram shown in Figure 7 and the pictorial representation of the molecular orbitals in Figure 6 indicate that there are some significant differences in the electronic structures of the two complexes. The increase in energy of the $8a_g$ MO for Pd vs Ni is the consequence of an increase in the ligand character of this MO from 20% to 40% which increases the antibonding interaction between the metal d_{z^2} and oxygen n_+ orbitals. There is also an increase in the metal d_{xz} contribution to the HOMO, from 4% for Ni to 16% for Pd. The two lowest unoccupied orbitals for both $Ni(acac)_2$ and $Pd(acac)_2$ are pure ligand orbitals. However, the energy gap between the HOMO and LUMO orbitals is smaller for the Pd than for the Ni complex.

The ZINDO-derived energies (eigenvalues) of the highest occupied molecular orbitals for $Pd(acac)_2$ can be compared to the results of previous ab initio PSHONDO (HONDO with pseudopotentials)[30] and DV $X\alpha$[31] calculations. The ZINDO and DV X_α methods provide a similar ordering and energy separation of the three highest occupied orbitals, with the next three molecular orbitals bunched at similar energies. The only significant difference between the computational results is the inversion of the $8a_g$ and $2b_{1u}$ orbitals in the PSHONDO calculation relative to the others. The several computational methods also provide similar descriptions of the bonding (eigenvectors) for the highest occupied MOs. However, some differences exist in the descriptions of MOs in which metal–ligand mixing is significant. For example, the ZINDO calculations show that the Pd-d_{xz} comprises 16% of the HOMO, while the PSHONDO calculations find 9% and DV $X\alpha$ 35%. The inclusion of reorganization energies via the DV $X\alpha$[31] and 2ph-TDA[21] methods is found to decrease the ionization energies of metal-localized orbitals (i.e., $8a_g$) relative to those of ligand-localized orbitals (i.e., $2b_{1u}$), resulting in inversions of some orbital energies when eigenvalues and ionization energies are compared.

The present limitations in the ZINDO parameterization schemes preclude a ZINDO study of $Pt(acac)_2$. However, its electronic structure has been calculated using the ab initio PSHONDO method and the results compared to those for $Pd(acac)_2$.[30] The resulting eigenvalues have been used to extend the ZINDO-derived correlation diagram to include the occupied orbitals of $Pt(acac)_2$ (Figure 7).[32] The most significant difference between the two complexes is the stronger admixing of ligand and metal orbitals for Pt vs Pd, as found to be the case in our comparison of Pd vs Ni. For example, the d_{xz} contribution to the $3b_{2g}$ HOMO in $Pt(acac)_2$, is double (18%) that calculated for $Pd(acac)_2$ (9%). The bonding and nonbonding MOs were found to be stabilized and the antibonding MOs slightly destabilized in $Pt(acac)_2$ versus $Pd(acac)_2$.

The ZINDO quantum chemical procedure also computes Mulliken atomic charges which provide a measure of the "covalency" of the $Ni(acac)_2$ and $Pd(acac)_2$ molecules.[27] In the case of $Ni(acac)_2$, the calculated charge on the metal (+0.68) is significantly less than that obtained from the conventional electron count for a d^8 metal(II) β-diketonate or from extended-Hückel[11] (+1.71) or SCF-MO[28] (+1.57) calculations. The value for $Pd(acac)_2$ (+0.63) is slightly less positive than that for Ni and is intermediate between those obtained for $Pd(acac)_2$ using the PSHONDO[30] (+0.97) and DV $X\alpha$[31] (+0.35) methods. The decrease in the magnitude of the positive charge on the metal center on going from the nickel to palladium derivative suggests that $Pd(acac)_2$ is more covalent than the nickel analogue, in agreement with the molecular orbital results (Figure 6). Di Bella et al.[30] report a further increase in covalency on going from $Pd(acac)_2$ to $Pt(acac)_2$. The Mulliken population analyses for $Ni(acac)_2$ vs $Pd(acac)_2$ and for $Pd(acac)_2$ vs $Pt(acac)_2$ indicate that the increased covalency is achieved by a larger ligand-to-metal charge transfer (LMCT) in the heavier metal complex.

To summarize the results of our electronic structure calculations for $Ni(acac)_2$ and $Pd(acac)_2$ and those of Di Bella et al.[30] for $Pd(acac)_2$ and $Pt(acac)_2$, increasing the atomic number of the

(28) Hirota, F.; Shubata, S. *J. Mol. Struct.* **1986**, *137*, 373–379.
(29) Fragalà, I.; Costanzo, L. L.; Ciliberto, E.; Condorelli, G.; D'Arrigo, C. *Inorg. Chim. Acta* **1980**, *40*, 15–24.
(30) Di Bella, S.; Fragalà, I.; Granozzi, G. *Inorg. Chem.* **1986**, *25*, 3997–4003.
(31) Casarin, M.; Vittadini, A.; Granozzi, G.; Fragalà, I.; Di Bella, S. *Chem. Phys. Lett.* **1987**, *141*, 193–197.
(32) For simplicity of comparing $Pt(acac)_2$ and $Pd(acac)_2$ orbitals, the same numerical order as used by Di Bella et al.[30] is used for both compounds. The direction of change (positive and negative) in orbital energies for Pt vs Pd is taken from Di Bella and co-workers. However, the $8a_g$ orbital is shown to lie above the $2b_{1u}$ for both $Pt(acac)_2$ and $Pd(acac)_2$, while this order is reversed by Di Bella and co-workers.

Table I. Calculated Absorption Maxima (λ_{max}), Oscillator Strengths (f), and Configuration Interaction (CI) of Excited Singlet States (S) of $Ni(acac)_2$

excited state[a]	state sym	λ_{max}, nm (f)	CI[b]	main character
S_1	B_{1g}	1352 (0.000)	86% $8a_g \rightarrow 6b_{1g}$	$d_{z^2} \rightarrow d_{xy}$
S_2	B_{3g}	982 (0.000)	86% $2b_{2g} \rightarrow 6b_{1g}$	$d_{xz} \rightarrow d_{xy}$
S_3	B_{2g}	939 (0.000)	96% $2b_{3g} \rightarrow 6b_{1g}$	$d_{yz} \rightarrow d_{xy}$
S_4	B_{1g}	732 (0.000)	56% $6a_g \rightarrow 6b_{1g}$	$d_{x^2-y^2} \rightarrow d_{xy}$
			45% $7a_g \rightarrow 6b_{1g}$	d_{z^2}, $d_{x^2-y^2} \rightarrow d_{xy}$
S_5	B_{1g}	292 (0.000)	53% $3b_{2g} \rightarrow 3b_{3g}$	$\pi_3 \rightarrow \pi_4$
			40% $2b_{1u} \rightarrow 2a_u$	
S_6	B_{2u}	283 (0.590)	53% $3b_{2g} \rightarrow 2a_u$	$\pi_3 \rightarrow \pi_4$
			36% $2b_{1u} \rightarrow 3b_{3g}$	
S_{16}	B_{2u}	213 (0.023)	34% $3b_{2g} \rightarrow 2a_u$	$\pi_3 \rightarrow \pi_4$
			46% $2b_{1u} \rightarrow 3b_{3g}$	
S_{17}	B_{3u}	209 (0.698)	92% $5b_{2u} \rightarrow 6b_{1g}$	$n_- \rightarrow d_{xy}$
S_{19}	B_{1u}	207 (0.163)	85% $8a_g \rightarrow 4b_{1u}$	$d_{z^2} \rightarrow$ Ni-p_z
			15% $8a_g \rightarrow 3b_{1u}$	$d_{z^2} \rightarrow$ Ni-p_z, C-p_z

[a] Higher energy excited singlet states having low or zero calculated oscillator strengths are omitted. [b] Only the major contributing pure configurations are listed.

Table II. Calculated Absorption Maxima (λ_{max}), Oscillator Strengths (f), and Configuration Interaction (CI) of Excited Singlet States (S) of $Pd(acac)_2$

excited state[a]	state sym	λ_{max}, nm (f)	CI[b]	main character
S_1	B_{1g}	377 (0.000)	71% $8a_g \rightarrow 6b_{1g}$	d_{z^2},$d_{x^2-y^2}$, O-$p_y \rightarrow d_{xy}$
			18% $3b_{2g} \rightarrow 3b_{3g}$	$\pi_3 \rightarrow \pi_4$
S_2	B_{3g}	332 (0.000)	76% $3b_{2g} \rightarrow 6b_{1g}$	$\pi_3 \rightarrow d_{xy}$
			23% $2b_{2g} \rightarrow 6b_{1g}$	$d_{xz} \rightarrow d_{xy}$
S_3	A_u	329 (0.000)	83% $8a_g \rightarrow 2a_u$	d_{z^2},$d_{x^2-y^2}$, O-$p_y \rightarrow \pi_4$
S_4	B_{3g}	328 (0.000)	81% $8a_g \rightarrow 3b_{3g}$	d_{z^2},$d_{x^2-y^2}$, O-$p_y \rightarrow \pi_4$
S_5	B_{2u}	309 (0.445)	74% $3b_{2g} \rightarrow 2a_u$	$\pi_3 \rightarrow \pi_4$
			21% $2b_{1u} \rightarrow 3b_{3g}$	
S_{12}	B_{2u}	222 (0.178)	20% $3b_{2g} \rightarrow 2a_u$	$\pi_3 \rightarrow \pi_4$
			66% $2b_{1u} \rightarrow 3b_{3g}$	
S_{14}	B_{1u}	216 (0.195)	62% $8a_g \rightarrow 3b_{1u}$	d_{z^2},$d_{x^2-y^2}$, O-$p_y \rightarrow$ Pd-p_z
			36% $8a_g \rightarrow 4b_{1u}$	
S_{15}	B_{3u}	215 (0.128)	55% $3b_{2g} \rightarrow 3b_{1u}$	$\pi_3 \rightarrow$ Pd-p_z
			26% $3b_{2g} \rightarrow 4b_{1u}$	
S_{16}	B_{3u}	210 (0.673)	94% $2b_{3g} \rightarrow 2a_u$	$d_{xy} \rightarrow \pi_4$

[a] Higher energy excited singlet states having low or zero calculated oscillator strengths are omitted. [b] Only the major contributing pure configurations are listed.

group 10(II) metal is found to result in an increase in metal-ligand covalency, an increase in the separation of the two highest occupied ($2b_{1u}$ and $3b_{2g}$) and lowest unoccupied ($2a_u$ and $3b_{3g}$) MOs, and a decrease in the separation between occupied and unoccupied orbitals (Ni and Pd only). The impact of these changes upon the optical spectra of these molecules will be described in the following section.

Optical Spectra. While the interpretation of ground state properties via quantum chemical calculations has become a relatively routine procedure, the use of electronic structure techniques to understand excited state properties in inorganic systems still presents challenging problems. The success of the ZINDO method in calculating the optical spectra of large transition-metal complexes such as ferrocene[14] and metalloporphines[33] encouraged us to undertake the present investigation. Briefly summarized, the ZINDO method calculates the energy, oscillator strength, and character (configuration interaction coefficients) of each electronic transition by first calculating the transition moments between occupied and unoccupied MOs to determine the "allowedness" of each transition, correcting transition energies for relaxation effects, and then allowing excited configurations to intermix via configuration interaction. The results of the ZINDO calculations will first be presented and compared with the observed spectra and then discussed in some detail.

ZINDO calculations on the acetylacetonate anion (acac) using the ligand geometries of $Ni(acac)_2$ predict a π,π^* excited singlet state at 288 nm ($f = 0.41$) with 98% of the excitation comprised of the $\pi_3 \rightarrow \pi_4$ (HOMO→LUMO) transition. This assignment is in agreement with an earlier assignment of the absorption maximum to a $\pi \rightarrow \pi^*$ ($\pi_3 \rightarrow \pi_4$) transition of the enolate ring using Hückel LCAO-MO[34] and PSHONDO[30] calculations. The calculated singlet state energy is also in agreement with the observed spectrum of Na(acac).[22]

The ZINDO-derived electronic transition energies, oscillator strengths, and dominant configurations for the six lowest excited singlet states and selected higher singlet states of $Ni(acac)_2$ are reported in Table I. The five lowest excited singlet states for $Ni(acac)_2$ all have zero calculated oscillator strengths. The first four arise from relatively pure d→d transitions with calculated wavelengths ranging from 1352 nm to 732 nm. The fifth excited singlet state (S_5) is a ligand-localized π,π^* state comprised of a configuration interaction between the nearly-degenerate highest occupied ($3b_{2g}$ and $2b_{1u}$) and lowest unoccupied ($2a_u$ and $3b_{3g}$) orbitals, involving the HOMO ($3b_{2g}$) → SLUMO ($3b_{3g}$) and SHOMO ($2b_{1u}$) → LUMO ($2a_u$) combinations. Configuration interaction between the same highest occupied ($3b_{2g}$ and $2b_{1u}$) and lowest unoccupied ($2a_u$ and $3b_{3g}$) orbitals involving instead the HOMO→LUMO and SHOMO→SLUMO transitions results in the first strong ($f = 0.590$) $\pi \rightarrow \pi^*$ transition at 283 nm (S_6) and a weak ($f = 0.023$) $\pi \rightarrow \pi^*$ transition at 213 nm (S_{16}). The next higher energy state with a large calculated oscillator strength ($f = 0.698$) is the essentially pure $n_- \rightarrow d_{xy}$ transition at 209 nm (S_{17}). A relatively weak S_{19} state ($f = 0.163$) is calculated at 207 nm and is predicted to have mainly a Ni-$d_{z^2} \rightarrow$ Ni-p_z character.

The ZINDO-derived properties of the lowest excited singlet states and selected higher singlet states of $Pd(acac)_2$ are reported in Table II. The four lowest singlet states for $Pd(acac)_2$ all have zero-calculated oscillator strengths. The S_1 and S_2 states include a mixture of metal d→d, ligand $\pi \rightarrow \pi^*$, and LMCT transitions. The S_3 excited singlet state is nearly a pure SHOMO→LUMO (MLCT) transition, while the S_4 state is mainly a SHOMO→SLUMO (MLCT) transition. As in the case of $Ni(acac)_2$, configuration interaction between the two highest occupied ($3b_{2g}$ and $2b_{1u}$) and two lowest unoccupied ($2a_u$ and $3b_{3g}$) ligand-localized orbitals in $Pd(acac)_2$ results in a strong ($f = 0.445$) $\pi \rightarrow \pi^*$ transition at 309 nm (S_5) and a weaker ($f = 0.178$) transition at 222 nm (S_{12}). The extent of configuration interaction is smaller and the calculated oscillator strengths are more nearly equal for S_5 and S_{12} than in the corresponding singlet states of $Ni(acac)_2$. In addition to the lower energy excited states, there is also a moderately strong ($f = 0.195$) metal "d→p" transition at 216 nm (S_{14}), a moderately strong ($f = 0.128$) LMCT state at 215 nm (S_{15}), and a very strong ($f = 0.673$) pure MLCT transition at 210 nm (S_{16}).

The calculated energies and oscillator strengths are shown as vertical bars in Figures 1 and 2. The agreement between the calculated and observed lowest energy allowed transitions for $Ni(acac)_2$ (283 vs 298 nm) and for $Pd(acac)_2$ (309 vs 326 nm) is quite good. ZINDO also correctly predicts the occurrence of several low energy forbidden d→d transitions for Ni but not for Pd and the occurrence of several allowed high energy ultraviolet (>220 nm) transitions for Pd but not for Ni.

Oscillator strengths for zero-order transitions are calculated using normal group theoretical considerations. The five lowest energy excited singlet states of $Ni(acac)_2$ (Table I) and the four lowest excited singlet states of $Pd(acac)_2$ (Table II) involve symmetry forbidden transitions and, as a consequence, have zero calculated oscillator strengths. The $3b_{2g} \rightarrow 2a_u$ and $2b_{1u} \rightarrow 3b_{3g}$ transitions of both $Ni(acac)_2$ and $Pd(acac)_2$ are symmetry allowed and thus the S_6 and S_{16} excited singlet states of $Ni(acac)_2$ and the S_5 and S_{12} excited singlet states of $Pd(acac)_2$ have large

(33) Edwards, W. D.; Zerner, M. C. *Can. J. Chem.* **1985**, *63*, 1763–1772.
(34) Barnum, D. W. *J. Inorg. Nucl. Chem.* **1961**, *21*, 221–237.

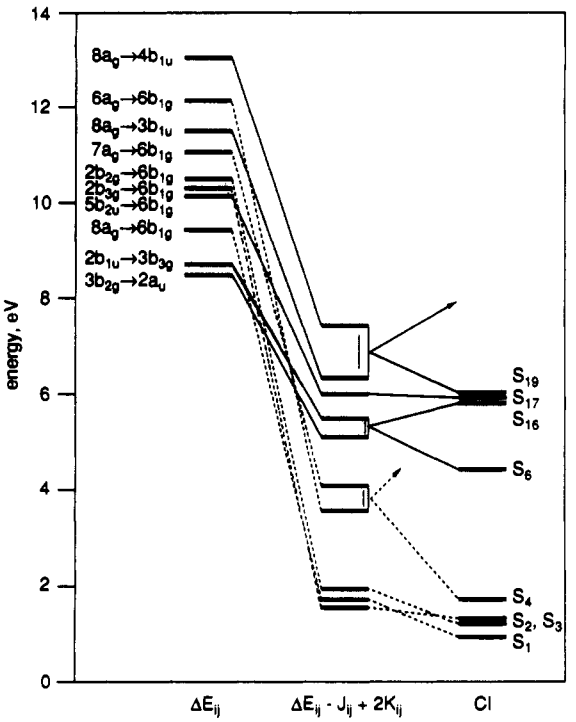

Figure 8. Platt diagram for Ni(acac)$_2$ displaying the molecular orbital energy differences (ΔE_{ij}), the pure configuration energies ($\Delta E_{ij} - J_{ij} + 2K_{ij}$) after correction for Coulomb (J) and exchange (K) repulsions, and the excited state energies after allowing for configuration interaction (CI). Solid lines connect allowed transitions and dashed lines connect forbidden transitions. Vertical lines designate strongly interacting configurations.

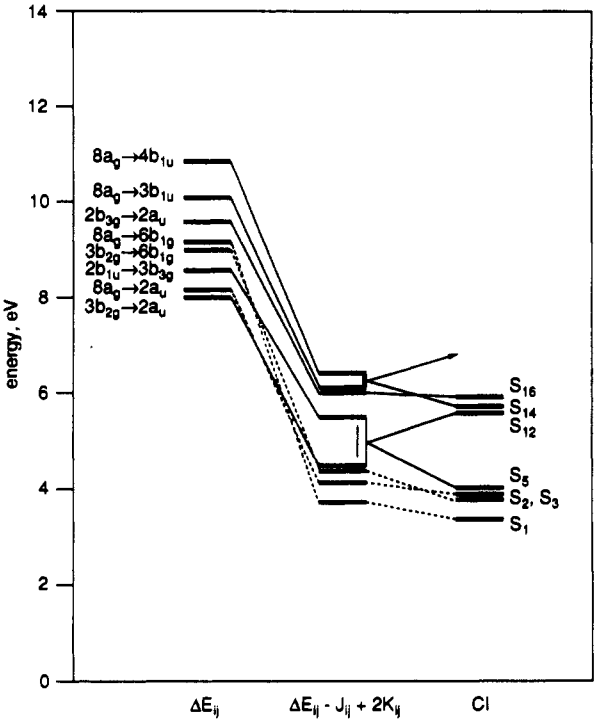

Figure 9. Platt diagram for Pd(acac)$_2$ displaying the molecular orbital energy differences (ΔE_{ij}), the pure configuration energies ($\Delta E_{ij} - J_{ij} + 2K_{ij}$) after correction for Coulomb (J) and exchange (K) repulsions, and the excited state energies after allowing for configuration interaction (CI). Solid lines connect allowed transitions and dashed lines connect forbidden transitions. Vertical lines designate strongly interacting configurations.

calculated oscillator strengths (Tables I and II). It should be noted that the ZINDO program does not include the vibronic coupling term in its Hamiltonian, thus it does not account for the stealing of intensity which occurs from nearby allowed transitions via vibronic coupling. Calculated oscillator strengths of zero, therefore, must only be taken as a prediction of low intensity ($\epsilon < 10^2$).

In addition to calculating the allowedness or intensity of a transition between molecular orbitals, ZINDO also computes the energy of the resulting excited configuration.[27] It does so by first computing the orbital energy difference (ΔE_{ij}) between the corresponding i and j molecular orbitals for each transition using the energies of occupied and unoccupied orbitals as displayed in Figure 7. The values of ΔE_{ij} are displayed schematically for Ni(acac)$_2$ and Pd(acac)$_2$ in Figures 8 and 9 at the left side of the Platt diagrams.[35] These virtual orbital energy differences grossly overestimate the actual transition energies due to the nature of the model Hamiltonian employed in the SCF-based electronic structure computations.[36] The Hartree–Fock-like operator contains Coulomb and exchange operators from only the electrons in occupied MOs. Thus, while electrons in occupied MOs "see" $n - 1$ electrons, the virtual orbitals see all n electrons.[36] This results in artificially high SCF energies for the unoccupied orbitals relative to the occupied orbitals.

The values of ΔE_{ij} for singlet to singlet transitions can be corrected by simply subtracting ($J_{ij} - 2K_{ij}$), where J_{ij} and K_{ij} are the two-center Coulomb and exchange integrals, respectively. The resulting values of $\Delta E_{ij} - (J_{ij} - 2K_{ij})$ for selected transitions are shown in the second column of Figures 8 and 9. For the singlet to singlet transitions of interest here, the Coulomb integral dominates the total relaxation energy and becomes particularly large when the occupied and unoccupied orbitals are localized on the same center, as is the case for the metal d→d transitions. For example, the 8a$_g$→6b$_{1g}$ transition of Ni(acac)$_2$ involves orbitals localized on the same center, namely the metal d_{z^2} and d_{xy} orbitals, and the values of J_{ij} (8.8 eV) and K_{ij} (0.6 eV) values for this transition are large. Consequently, the ZINDO-derived pure singlet excited configuration energy for this transition is located in the visible region (1.7 eV, 737 nm) instead of the far ultraviolet region predicted by the orbital energy difference (ΔE_{ij} = 9.4 eV, 132 nm). In contrast, the 3b$_{2g}$→2a$_u$ ($\pi_3 \rightarrow \pi_4^*$) transition involves orbitals whose electrons are delocalized over a mixed ligand-metal framework and thus the values of J_{ij} (4.2) and K_{ij} (0.4) are relatively small and the corrected pure excited singlet configuration is still found in the ultraviolet region (5.2 eV, 239 nm vs ΔE_{ij} = 8.5 eV, 146 nm).

An important consequence of the larger Coulomb and exchange integrals for localized d→d vs delocalized $\pi \rightarrow \pi^*$ transitions is that corrected transition energies, $\Delta E_{ij} - J_{ij} + 2K_{ij}$, for the latter are smaller than for the former. As seen in Figures 8 and 9, the lowering of the d→d vs $\pi \rightarrow \pi^*$ transition energies is smaller in the case of Pd(acac)$_2$ than in the case of Ni(acac)$_2$. The 8a$_g$→6b$_{1g}$ transition of Pd(acac)$_2$ involves orbitals having a larger degree of metal-d and oxygen-p electron delocalization than is the case for Ni(acac)$_2$. Consequently, the values of J (6.1) and K (0.3) for this d→d transition of Pd(acac)$_2$ are less than those for Ni(acac)$_2$ and the pure excited singlet configuration of Pd(acac)$_2$ is calculated to occur at 338 nm (3.7 eV) instead of 737 nm (1.7 eV) as calculated for Ni(acac)$_2$.

The third step needed to calculate accurately the electronic absorption spectra of the group 10(II) β-diketonates is the computation of configuration interaction coefficients. In theory, if an excited state were comprised of only one pure configuration, the pure excited singlet configuration energy ($\Delta E_{ij} - J_{ij} + 2K_{ij}$) would be the energy of the excited singlet state. This is approximately the case for states dominated by a single configuration such as S$_3$ and S$_{17}$ for Ni(acac)$_2$ and S$_{16}$ for Pd(acac)$_2$. However, as shown in Tables I and II, all of the other singlet

(35) Platt, J. R. *J. Chem. Phys.* **1950**, *18*, 1168–1173.
(36) Pople, J. A.; Beveridge, D. L. *Approximate Molecular Orbital Theory*; McGraw-Hill: New York, 1970.

excited states are comprised of mixtures of two or more configurations (note that only the major configurations are included in the tables).

The means by which pure configurations intermix (configuration interaction) and the magnitude of the interaction energy (H) are described by the integral

$$H_{ij,i'j'} = \int \Phi_{ij} \mathcal{H} \Phi_{i'j'} \, d\tau \qquad (1)$$

where $\mathcal{H}$ is the Hamiltonian operator and Φ is the pure excited configuration for the $i \rightarrow j$ (or $i' \rightarrow j'$) transition (eq 1). The Hamiltonian operator transforms as the totally symmetric representation (i.e., the symmetry of $\mathcal{H}$ is A_g). As a rule, the product ($\Phi_{ij} \cdot \Phi_{i'j'}$) can only equal A_g when the symmetries of the two configurations are the same. Thus, in order for the integral in eq 1 to be nonvanishing and, consequently, for configuration interaction to occur, the symmetries of the pure configurations (Φ_{ij} and $\Phi_{i'j'}$) must be the same. The result of this configuration interaction is to produce two new excited states of mixed Φ_{ij} and $\Phi_{i'j'}$ character, where the energy difference between the two excited singlet states is greater than that between the two pure configurations. For example, the symmetry of the HOMO→LUMO configuration of Ni(acac)$_2$ is B_{2u} ($b_{2g} \cdot a_u$), as is the symmetry of the SHOMO→SLUMO excitation ($b_{1u} \cdot b_{3g}$). Therefore, the HOMO→LUMO and SHOMO→SLUMO transitions of Ni(acac)$_2$ mix via configuration interaction and produce the S_6 and S_{16} excited states having both HOMO→LUMO and SHOMO→SLUMO character.

In addition to symmetry, the extent of CI mixing is dependent upon several factors, the most important of which is the energetic proximity of the configurations. Considering, for example, the configuration of B_{2u} symmetry in Ni(acac)$_2$, the $3b_{2g} \rightarrow 2a_u$ (5.2 eV) and $2b_{1u} \rightarrow 3b_{3g}$ (5.5 eV) pure configurations are close in energy (Figure 8) and interact strongly, but interact only weakly (<5%) with the higher energy B_{2u} configurations [the $2b_{2g} \rightarrow 2a_u$ (6.4 eV) and $6b_{3u} \rightarrow 6b_{1g}$ (6.8 eV)] which are not shown in Figure 8. Consequently, the major components of the lowest energy B_{2u} excited singlet states (Table I) are the $3b_{2g} \rightarrow 2a_u$ and $2b_{1u} \rightarrow 3b_{3g}$ configurations, with S_6 having a 53%:36% and S_{16} having a 34%:46% mixture of the former and latter configurations, respectively. Comparison of the same two B_{2u} configurations of Pd(acac)$_2$ (Figure 9) shows that the $3b_{2g} \rightarrow 2a_u$ (4.5 eV) and $2b_{1u} \rightarrow 3b_{3g}$ (5.5 eV) configurations are not as close in energy as they were in Ni(acac)$_2$, therefore the interaction between the two configurations is not as strong. As shown in Table II, the resulting S_5 excited singlet state of Pd(acac)$_2$ is characterized by a 74%:21% mixture and the S_{12} excited state is characterized by a 20%:66% mixture of the $3b_{2g} \rightarrow 2a_u$ and $2b_{1u} \rightarrow 3b_{3g}$ configurations, respectively.

Configuration interaction is also known to affect the intensities of transitions to the excited singlet states of a molecule but in a manner that is not well understood. When two pure configurations are close in energy and, therefore, when configuration interaction takes place, the "sharing" of intensity between the two configurations or the "stealing" of intensity from one configuration by the other can occur. A stronger configuration interaction results in a greater transferring of intensity. The result is the production of two excited states, one of strong intensity and one of weak intensity. Using the B_{2u} excited configurations again as an example, the $3b_{2g} \rightarrow 2a_u$ and $2b_{1u} \rightarrow 3b_{3g}$ configurations of Ni(acac)$_2$ are closer in energy, have a stronger configuration interaction, and thus have a greater transferring of intensity than do the same configurations of Pd(acac)$_2$. Consequently, the resulting Ni(acac)$_2$ excited states, S_6 (f = 0.590) and S_{16} (f = 0.023), have very different intensities while the Pd(acac)$_2$ excited states, S_5 (f = 0.445) and S_{12} (f = 0.195), have more nearly equivalent intensities.

It should be noted that this interpretation of the optical spectra arising from the nearly-degenerate pairs of occupied ($3b_{2g}$ and $2b_{1u}$) and unoccupied ($2a_u$ and $3b_{3g}$) orbitals is highly analogous to the four level model developed by Platt[35] for the interpretation of the optical spectra of aromatic hydrocarbons and later employed by Gouterman[37] and Edwards and Zerner[33] for the interpretation of the optical spectra of metalloporphines. Platt observed that when the pairs of occupied and unoccupied MOs have similar energies (the "round field" case), configuration interaction is significant and results in a large energy separation in the resulting optical transitions and a stealing of intensity by one transition from the other. When strong covalent interactions remove the degeneracy of the pairs of occupied and unoccupied MOs (the "long field" or "strong field" case), configuration interaction is less important and "intensity stealing" does not occur to as great an extent. Using Platt's categories, Ni(acac)$_2$ is more nearly a "round field" molecule and Pd(acac)$_2$ a "long field" molecule.

While configuration interaction involving the four B_{2u} excited configurations has the most noticeable effect upon the observed optical spectra, the energies and intensities of other singlet states are also affected by configuration interaction. Among the other significant effects of CI are the lowering of the energies of S_4 and S_{19} for Ni(acac)$_2$ (Figure 8) and of S_{14} for Pd(acac)$_2$ (Figure 9). S_4 may be responsible for the 644 nm maximum and S_{19}, along with S_{17}, for the end absorption observed in the optical spectrum of Ni(acac)$_2$ in ethanol solution (Figure 1). Similarly, S_{16} may be responsible for one of the shoulders observed below 250 nm for Pd(acac)$_2$ (Figure 2).

Extending this analysis to Pt(acac)$_2$, the increase in covalency for the series Ni < Pd < Pt should make Pt(acac)$_2$ more nearly a "long field" case than Pd(acac)$_2$. An increase in the separation of the pairs of occupied and unoccupied MOs should result in a decrease in mixing of $3b_{2g} \rightarrow 2a_u$ and $2b_{1u} \rightarrow 3b_{3g}$ configurations for Pt vs Pd. We tentatively assign the 344 nm absorption band and one of the higher energy bands in Figure 3 to the two relatively pure, allowed $\pi \rightarrow \pi^*$ transitions. This assignment is supported by the observation[5] that the band maxima shift to longer wavelength when the methyl groups of the ligand are replaced with phenyl groups, which extend the π-conjugation.

Concluding Remarks. The results of this investigation serve to elucidate the origins of the markedly different appearance of the optical spectra of Ni(acac)$_2$, Pd(acac)$_2$, and Pt(acac)$_2$ (Figures 1–3) originally noted by Holm and Cotton[9] three decades ago. These differences have their origins in changes in the electronic structure of the complexes; namely, the increase in metal–ligand covalency with increasing atomic number. This increase is manifested in both a decrease in the calculated Mulliken atomic charge on the metal and an increase in mixing of ligand and metal character in some of the molecular orbitals, most notably the highest occupied π_3 ($3b_{2g}$) and d ($8a_g$ and $3b_{2g}$) orbitals (Figure 6). As a consequence the energies of these orbitals are raised with respect to those of the other occupied frontier orbitals (Figure 7). These changes in electronic structure in turn affect the appearance of the optical spectrum. The increased separation of the pairs of highest occupied and lowest unoccupied π-orbitals with increasing atomic number results in decreased configuration interaction between the transitions connecting these states (Figures 8 vs 9 and Tables I and II) and hence decreased borrowing of intensity from one of these transitions by the other. Increased mixing of metal d-orbitals with ligand orbitals results in a smaller relaxation energy for the d→d transitions in Pd vs Ni (Figures 8 vs 9), resulting in the "disappearance" of d→d transitions for Pd.

Comparison of our assignment of the optical spectrum of Ni(acac)$_2$ to that of Cotton and Wise[12] provides some instructive contrasts. Since the extended-Hückel method does not allow for configuration interaction, it is not surprising that the allowed 298 nm absorption band was attributed to two overlapping $\pi \rightarrow \pi^*$ transitions rather than a single transition resulting from strong

(37) Gouterman, M. P. *J. Mol. Spectrosc.* **1961**, *6*, 138–163.

configuration interaction. While both methods assign weak visible absorption bands to d→d transitions, the extended-Hückel method places the energy of the filled d orbitals above the highest occupied ligand orbitals, while this order is reversed by both ZINDO and previously reported ab initio calculations. Furthermore, while the traditional explanation for the absence of d→d absorption bands in the spectra of $Pd(acac)_2$ and $Pt(acac)_2$ is based on the lowering of the filled d-orbitals below the filled ligand orbitals, both ZINDO and ab initio calculations indicate that the energy of the highest occupied d-orbital ($8a_g$) in fact increases with increasing atomic number (Figure 7).

The present study illustrates the utility of the ZINDO algorithm in interpreting the optical spectra of transition metal complexes in which the transition metal is changed while the ligand is constant. Our complementary studies of Pd(II) and Pt(II) bis-(β-diketonates) in which the metal is constant and the conjugation of the ligand varied will be reported subsequently.

Acknowledgment. The authors thank J. D. Oxman and L. D. Boardman of 3M Corp. for attracting our attention to the photochemistry and spectroscopy of platinum(II) β-diketonates and 3M for providing partial funding for this project.

Supplementary Material Available: Tables of eigenvalues, eigenvectors, and symmetries for $Ni(acac)_2$ and $Pd(acac)_2$ frontier orbitals, Mulliken atomic orbital populations for $Ni(acac)_2$ and $Pd(acac)_2$, formal charges for $Ni(acac)_2$, $Pd(acac)_2$, and acetylacetonate anion, oscillator strengths, energy differences for pure configurations, and corrections for Coulomb and exchange integrals for $Ni(acac)_2$ and $Pd(acac)_2$ (7 pages). Ordering information is given on any current masthead page.